Gaussian Markov Random Fields for Localizing Reinforcing Bars in Concrete Infrastructure

Karthick Thiyagarajan*, Sarath Kodagoda, Linh Van Nguyen & Sathira Wickramanayake

Centre for Autonomous Systems, University of Technology Sydney, Australia.
E-mail: Karthick.Thiyagarajan@uts.edu.au*

Abstract -

Sensor technologies play a significant role in monitoring the health conditions of urban sewer assets. Currently, the concrete sewer systems are undergoing corrosion due to bacterial activities on the concrete surfaces. Therefore, water utilities use predictive models to estimate the corrosion by using observations such as relative humidity or surface moisture conditions. Surface moisture conditions can be estimated by electrical resistivity based moisture sensing. However, the measurements of such sensors are influenced by the proximal presence of reinforcing bars. To mitigate such effects, the moisture sensor needs to be optimally oriented on the concrete surface. This paper focuses on developing a machine learning model for localizing the reinforcing bars inside the concrete through non-invasive measurements. This work utilizes a resistivity meter that works based on the Wenner technique to obtain electrical measurements on the concrete sample by taking measurements at different angles. Then, the measured data is fed to a Gaussian Markov Random Fields based spatial prediction model. The spatial prediction outcome of the proposed model demonstrated the feasibility of localizing the reinforcing bars with reasonable accuracy for the measurements taken at different angles. This information is vital for decision-making while deploying the moisture sensors in sewer systems.

Keywords -

Concrete sewer; Electrical resistivity; Gaussian Markov Random Fields; Localizing; Non-invasive; Reinforcing bars; Spatial prediction; Wenner technique.

1 Introduction

Recently, robotic systems are largely viewed by scientists as a promising tool to navigate, explore and measure environmental health of hostile areas [1]. One such area is an urban sewer system, where long-term direct human exposure can cause occupational health hazards [2]. Exploiting robotic inspections in such infrastructures not only requires hi-tech robots but also advanced sensing technologies in order to provide credible information about the sewer assets. In this context, this work focuses on utilizing the sensor data and provide meaningful information for pertinent decision-making.

The underground sewer pipes are deteriorating mainly due to microbial induced concrete corrosion [3, 4]. This raises concerns among water utilities around the globe as the sewer asset rehabilitation costs are at an estimated annual value of over $100 millions [5, 6]. Presently, water utilities use data-driven machine learning models for estimating corrosion [7]. In such models, surface moisture conditions of the concrete sewers can be used as an observation for improved prediction [8, 9]. So, a new robust sensing technology was developed by us in collaboration with four water utilities in Australia. This technology estimates surface moisture levels based on non-invasive electrical resistivity measurements.

The technology was deployed and tested in a sewer pipe belonging to Sydney Water in Sydney, Australia. This evaluation demonstrated sensing feasibility under aggressive sewer conditions and capabilities for long-term moisture monitoring operations. However, the sensor measurements can be influenced by the reinforcing bars (rebars) inside the concrete and hence requiring onsite calibration. Therefore, the research problem is to determine the location and orientation of rebar embedded in concrete by using the same sensor rather than having to rely on expensive sensors such as ground penetratin radars. This allows appropriate localization of sensor installations to improve the reliability of moisture estimations.

In this paper, we propose a discretely indexed Gaussian Markov Random Fields (GMRFs) based data-driven machine learning model for spatially localizing the rebar embedded in concrete using electrical resistivity measurements. The proposed machine learning method is a computationally efficient alternative to the non-parametric Gaussian Process (GP) based models. In this work, we employ resistivity meter to perform non-invasive measurements of electrical resistivity variation on the concrete sample by utilizing four probe Wenner technique. The measurements were taken at different spatial location of the concrete sample by placing the resistivity meter on the concrete surface at different angles with respect to the rebar. Then, the measured data obtained from each angle is fed to the

GMRF model for experimental investigations.

The remainder of the paper is structured as follows: Section 2 elucidates the sensing technique and procedures followed for data collection. Section 3 formulates the theoretical considerations for spatial prediction. Section 4 presents the experimental results with analysis. Section 5 discusses the limitations of the work. Finally, Section 6 concludes the proposed work with future prospects.

2 Electrical Resistivity Measurements

An electrical resistivity meter was developed in the laboratory to measure surface electrical resistivity variations on the concrete. This device performs non-invasive measurements based on the Wenner technique [10], which uses four electrodes with an equal spacing distance between them. The two outer electrodes inject electrical current into the concrete material whereas the two inner electrodes measure the electrical potential differences. Then, the electrical resistivity of the concrete on the surface of interest can be determined by using Equation 1:

$$\rho = 2\pi a\left(\frac{V}{I}\right) \tag{1}$$

where ρ is the electrical resistivity of the concrete denoted in terms of kΩcm, a = 40mm is the spacing between the two electrodes, V is the electrical voltage signal measured by the inner two electrodes and I is the electrical current injected by the outer two electrodes.

The developed device is compact and works on the open-source electronic prototyping platform (Arduino Nano). It was evaluated on the benchmark scale and it produced measurements as desired. More information on the development of this resistivity meter is available in [11].

A concrete of thickness: 10 cm, width: 35 cm and length: 35 cm was made with a rebar having width: 1.2 cm, height: 1.2 cm and length: 30 cm was embedded into the concrete material at a 2 cm depth from the top surface of the concrete. This concrete was divided into several cells to perform measurements in those cells. Totally, the concrete was partitioned into 49 cells and each cell had a dimension of $4cm^2$. The rebar runs through the column 4 of the (7×7) partitions. Electrical resistivity measurements in each cell were obtained by placing the inner two electrodes of the sensor at different angles. For each angle, two sets of data were taken in each cell.

3 Modelling for Spatial Prediction

3.1 Gaussian Markov Random Fields

GMRFs are a discretely indexed Gaussian Fields, which can be achieved through the observations of random variables in the spatial process [12]. It incorporates Gaussian Processes and also satisfies Markovian property [13]. This makes GMRFs a computationally efficient alternative to GP [14].

Let $s = (s_1, s_2, s_3, ..., s_n)^T$ with $s \sim \mathcal{N}(\mu, Q^{-1})$ referring to GMRFs given by the mean μ and a symmetric and positive definite precision matrix Q that represents the convex polytope in $\mathbb{R}^d$ ($\mathbb{R}$ denotes real numbers), and an inverse of the GP covariance matrix, $\sum$ [12, 15]. So, the density of s will be of the mathematical form as given in Equation 2:

$$p(s) = (2\pi)^{-\frac{n}{2}}\left(det(Q)\right)^{\frac{1}{2}} exp\left\{-\frac{1}{2}(s-\mu)^T Q(s-\mu)\right\} \tag{2}$$

The salient feature of the Markovian property is that the full conditional distribution of s_i $(1 \leq i \leq n)$ is only dependent on the elements set of the neighbourhood structure of the process and it is given by Equation 3

$$p(s_i|s_{-i}) = p(s_i|s_{Ni}) \tag{3}$$

where s_{-i} represents the elements in s apart from the element s_i, and s_{Ni} denotes the neighbourhood elements of s_i. Therefore, it is established that in the case of given neighbourhood elements, s_i element is independent on all other elements in s with the exception of the element s_{Ni}, which defines the conditional independence as $s_i \perp s_{-i,Ni}|s_{Ni}$ ($\perp$ denotes the independence of two variables) for $1 \leq i \leq n$. According to [12], μ is not related to pairwise conditional independence properties of s and therefore, afore stated characteristic is limited to the precision matrix Q. Generally, if s_i and s_j are conditionally independent, $s_i \perp s_{-j}|s_{-i,j}$ is equivalent to $Q_{ij} = 0$. This condition give rise to $Q_{ij} \neq 0$ when $j \in \{i, N_i\}$ and deduce the sparsity of Q that results significantly in computation performance.

3.2 Spatial Field Model by way of GMRFs

Let the finite set of spatially observed locations be $\psi = (\psi_1^T, \psi_2^T, \psi_3^T, ..., \psi_n^T)^T$. Each spatially observed location in ψ comprise of one electrical resistivity measurement data and consider $x(\psi) = (x(\psi_1), x(\psi_2), x(\psi_3), ..., x(\psi_n))^T$ as the vector of measurements in the spatial field [12]. In this work, the model utilized is similar to [15, 14], which is a summation of a large scale component, a random field and an identically distributed noise. The model is mathematically defined in Equation 4:

$$x(\psi) = \zeta(\psi)\beta + s(\psi) + \epsilon(\psi) \tag{4}$$

where $\zeta(\psi)\beta = \mathbb{E}(x(\psi))$ is the expectation of $(x(\psi))$ and $\mathbb{E}(\cdot)$ defines the expectation operator. $\zeta(\psi)$ is the covariates

determined at spatial location ψ and β is the vector of mean parameters. s is a GMRFs with a n zero mean vector and a $n \times n$ precision matrix Q. $\epsilon(\psi)$ is the measurement noise with $\mu = 0$ and a known covariance matrix $\sigma_\epsilon^2 I_\epsilon$ at spatial locations ψ_i $(1 \leq i \leq n)$, where σ_ϵ^2 is assumed to be known and I_ϵ is the identity matrix, $n \times n$.

As in [16], the GMRF can precisely work as a GP when the continuous domain stochastic partial differential equations (SPDE) possess a solution with Matern covariance function [12], which is mathematically given by Equation 5:

$$cov(\gamma) = \frac{\sigma^2}{\Gamma(v)2^{v-1}}(\kappa\gamma)^v K_v(\kappa\gamma) \tag{5}$$

where γ indicates the Euclidean distance between the spatial locations, $\gamma = \|v_i - v_j\|$. The term σ^2 denotes the marginal variance and the term κ implies spatial parameters with v as the Matern smoothness and K_v represents the modified Bessel function [12]. The term $\zeta(\psi)\beta$, in this case denotes the mean function in the context of GP [17, 18].

3.3 Sensor Data Modelled by GMRFs Using SPDE Approach

The SPDE approach formulated by [19] demonstrates computational effectiveness while used in the spatial process. This approach incorporates finite element method [20] to focus the SPDE onto a basis representation, which includes piece-wise linear basis functions described by a triangulation that pertains to the interested regions [12]. Assuming that the spatial process $s(p)$ is observed at N locations where $p = (p_1^T, p_2^T, p_3^T, ..., p_n^T)^T$, then the initial vertices of the triangle are set at those spatial locations. Further, in order to achieve spatial prediction, more vertices of the triangles are added to realize a large triangulation.

The GMRF model is developed on the basis function representation for the given triangulation of the domain Q [12]. Therefore, $s(p)$ is given as in Equation 6:

$$s(p) = \sum_{i=1}^{n} f_i(p) w_i \tag{6}$$

where $\{f_i(p)\}$ denotes the basis functions that are piece-wise linear on each triangle [12]. In the i^{th} vertex of the mesh, $f_i(p)$ of the functions $\{f_i(p)\}$ is 1, and 0 for all other vertices. The term $\{w_i\}$ denotes the Gaussian distributed weight. At each triangle vertex i, the value of the spatial field is given by $\{w_i\}$ [12]. Thus, the SPDE approach incorporating finite element method establishes the link between the GP and GMRFs with feasible computation efficacy. The precision matrix Q of size $n \times n$ is determined by computing the Equation 7:

$$Q = \tau^2(\kappa^4 D + 2\kappa^2 H + H D^{-1} H) \tag{7}$$

where τ controls the variance, D and H are the $n \times n$ matrices with $D_{ij} = \langle f_i, f_j \rangle$ and $H_{ij} = \langle \Delta f_i, \Delta f_j \rangle$.

The total number of triangulation vertices defines the dimension of Q in the region of interest. Thus, Q can be seen as a function of κ and τ. Lets define the hyper-parameter vector as $\Phi = (\log(\tau), \log(\kappa))$. Now, it can be said that the sparse property of Q is embraced by the GMRFs representation built by the linear basis functions. The inherent random field at the n vertices of the triangulation is defined by GMRFs with μ as

$$s|\Phi \sim \mathcal{N}(\mu, Q^{-1}) \tag{8}$$

In the interest of mapping between the basis function representation located at n vertex of the triangulation and random field at resistivity meter locations having N dimension, let us consider the projector matrix as B, whose size is $N \times n$. B projects the modelled inherent random field at the vertices of the triangulation to the data locations.

In reference to the spatial field model presented in the preceding section, the measurements at N locations of the spatial field can be given by Equation 9:

$$x|s, \Phi, \beta, \sigma_\epsilon^2 \sim \mathcal{N}(\zeta(p)\beta + Bs, \sigma_\epsilon^2 I_N) \tag{9}$$

where $\zeta(p)$ refers to $N \times q$ matrix of covariates, β and Φ are the estimated parameters of the maximum likelihood approach [18], I_N refers the identity matrix $N \times N$.

If all the model parameters are learned, the joint distributions of x and s are calculated by adopting the technique in [21, 12], which is given by Equation 10:

$$s|x, \Phi, \beta, \sigma_\epsilon^2, B \sim \mathcal{N}\left(\begin{bmatrix} 0 \\ \zeta(p)\beta \end{bmatrix}, \begin{bmatrix} Q^{-1} & Q^{-1}B^T \\ B^T Q^{-1} & \sigma_\epsilon^2 I + BQ^{-1}B^T \end{bmatrix} \right) \tag{10}$$

The full conditional distribution of s given by x is also Gaussian with respect to probabilistic theory [12]. By using block-wise inversion approach [22] and the Schur complement, the Gaussian expressed in Equation 10 can be mathematically written as in Equation 11:

$$s|x, \Phi, \beta, \sigma_\epsilon^2, B \sim \mathcal{N}\left(\mu_{s|x}, Q_{s|x}^{-1}\right) \tag{11}$$

where $\mu_{s|x}$ denotes the vector of posterior means and the term $Q_{s|x}$ denotes the posterior Q. They are given as follows:

$$\mu_{s|x} = \zeta(\psi)\beta + Q_{s|x}^{-1}(\sigma_\epsilon^2 I_N)^{-1}(x - \zeta(p)\beta) \tag{12}$$

$$Q_{s|x} = Q + B^T(\sigma_\epsilon^2 I_N)^{-1}B \quad (13)$$

Equation 12 factorizes the sparse matrix $Q_{s|x}$. However, $Q_{s|x}$ is not dependent on the collection of sensor measurements [15, 12].

4 Experimental Results

4.1 GMRFs Spatial Prediction Performance

This section investigates the spatial prediction performance of the GMRFs model. In this regard, this evaluation was carried out by placing the resistivity meter at an angle 90° and three sets of data were taken in the 49 partitions. Among the 49 partitions, 20 were used for training the GMRFs model and 29 were used for testing. The spatial prediction results for the three different datasets are shown in Figure 1, Figure 2 and Figure 3.

In order to evaluate the spatial prediction performance efficacy of the GMRFs model, Mean Absolute Error (MAE) and Root Mean Square Error (RMSE) were used as metrics, which was computed based on the data of measured values and the predicted values. Table 1 tabulates the computed metric values for the three different datasets, where it can be observed that the MAE and RMSE are reasonably low and therefore, the results indicate that the GMRFs model can be utilized for localizing the rebar.

4.2 GMRFs Spatial Predictions for Measurements Obtained from Different Angles

This section presents the results of the GMRFs predictions for localizing the rebar based on non-invasive

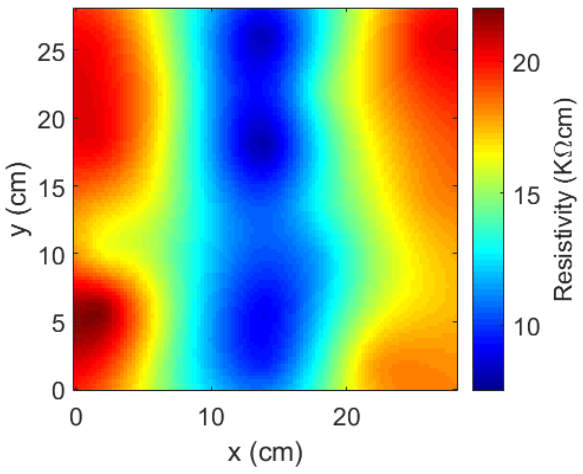

Figure 1. Dataset-1: Spatial prediction using GMRFs by taking resistivity measurements at 90°.

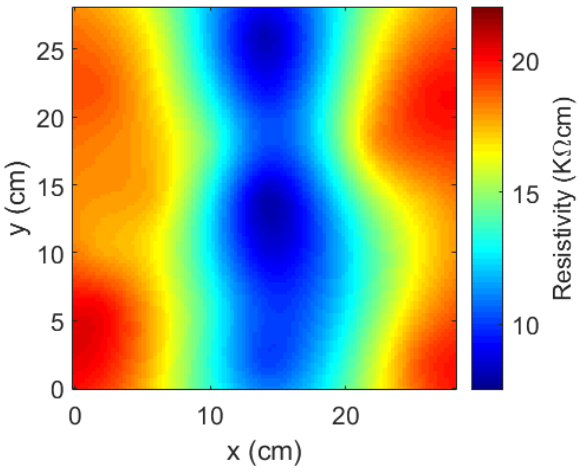

Figure 2. Dataset-2: Spatial prediction using GMRFs by taking resistivity measurements at 90°.

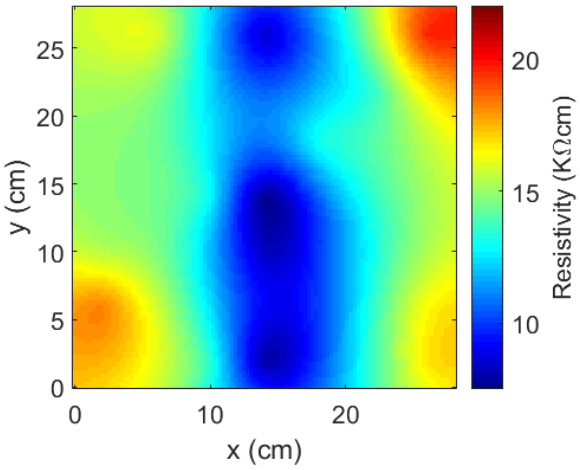

Figure 3. Dataset-3: Spatial prediction using GMRFs by taking resistivity measurements at 90°.

Table 1. GMRFs Spatial Prediction Performance

Datasets	MAE (kΩcm)	RMSE (kΩcm)
Dataset-1	0.50	1.69
Dataset-2	0.61	1.60
Dataset-3	0.28	1.37

electrical resistivity measurements. The measurements were taken by placing the resistivity meter at different angles such as 0°, 30°, 45°, 60° and 90°. The angle 0° is perpendicular to the rebar whereas the angle 90° is parallel to the rebar.

Figure 4 shows the spatial prediction for the measurements taken at an angle 0°, where it can be observed that area of low resistivity denotes the presence of rebar. Similarly, Figure 5 shows the spatial prediction for the measurements taken at an angle 30°, Figure 6 shows the spatial prediction for the measurements taken at an angle 45°, Figure 7 shows the spatial prediction for the measurements taken at an angle 60° and Figure 8 shows the spatial prediction for the measurements taken at an angle 90°.

From the figures showing the spatial prediction using GMRFs, the low resistivity area represents the influence of the rebar located inside the concrete. It can be said that the measurements taken at different angles such as 0°, 30°, 45°, 60° and 90° can be utilized to locate the rebar embedded in the concrete through GMRFs based spatial prediction model. This information of rebar placement can be used for optimal moisture sensor installations. However, it can be observed from the Figure 4 that the measurements taken at the angle 0° has less rebar influence compared to other angles.

5 Discussion

In the reported work, we performed electrical resistivity measurements on the concrete that has a rebar at 2 cm depth from the top concrete surface. In order to locate the rebar inside the concrete, whose rebar is placed at different depths lower than 2 cm, modifications need to be done in the sensing technique by changing the

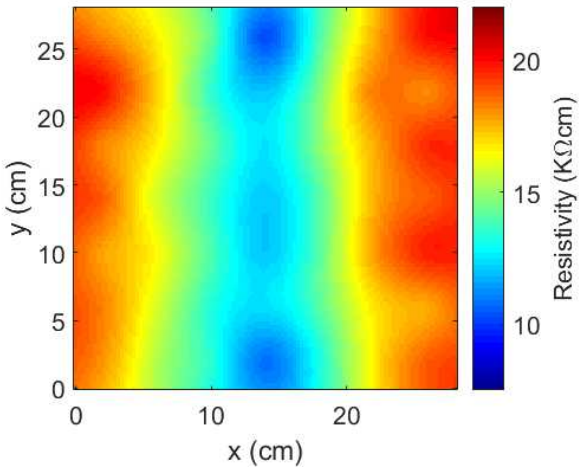

Figure 4. GMRFs prediction at 0° measurements.

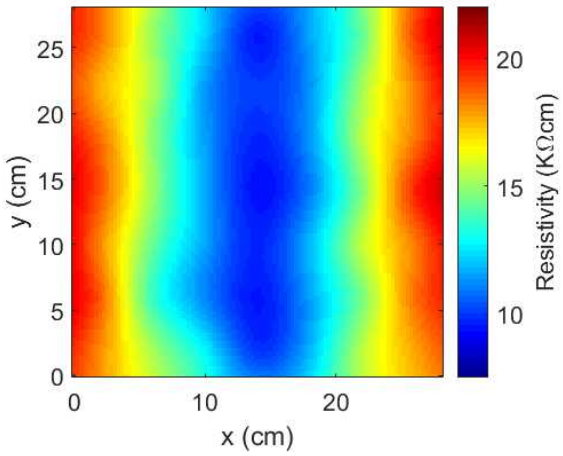

Figure 5. GMRFs prediction at 30° measurements.

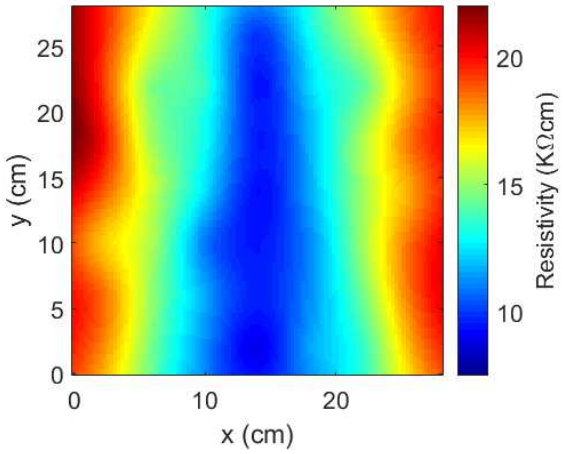

Figure 6. GMRFs prediction at 45° measurements.

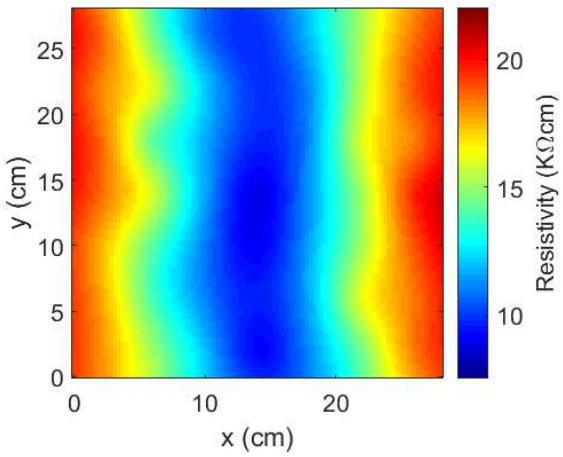

Figure 7. GMRFs prediction at 60° measurements.

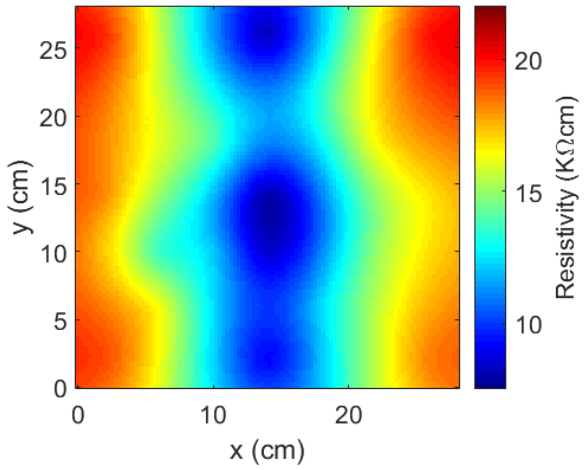

Figure 8. GMRFs prediction at 90° measurements.

operating frequency. Presently, the device used in this work is set to perform measurements with 40 Hertz. However, it is possible to change the frequency of the device based on the application. Also, the rebars that are located near the measuring surface of the concrete only has influence during moisture measurements for 40 Hertz. Higher the operating frequency higher is the penetration depth of electrical signals into the concrete.

With the operating frequency of 40 Hertz, given the unknown conditions of the rebar at sewer pipes, the electrical resistivity measurements taken at different angles through GMRFs spatial prediction model can shed light on the rebar location. Therefore, this information is vital to place the electrical resistivity meter for surface moisture estimation in sewer systems.

6 Conclusions

This paper proposed a machine learning model using GMRFs for localizing the rebar in concrete infrastructures. In this context, the work reported has led to the following three major contributions:

- We experimentally demonstrated that non-invasive electrical resistivity measurements based on Wenner technique has influence to the embedded rebar of the concrete and henceforth, the measured data can be utilized to determine the rebar location.
- The proposed GMRFs model for spatial prediction based on electrical resistivity measurements has produced satisfactory results and the statistical evaluation results computed from three different datasets demonstrate that the spatial prediction performance of the GMRF model is reasonably accurate and can be used for localizing the rebar.
- GMRFs spatial prediction based on the measurements at different angles such as 0°, 30°, 45°, 60° and 90° demonstrated that rebar can be identified irrespective of measurement angles. However, there was less influence of rebar when the measurements were taken perpendicular to the rebar.

Overall, the proposed work can improve the way surface moisture conditions are quantified inside the concrete sewer systems. In the future, the reported work will be extended to perform measurements on larger concrete having rebar meshes. Then, in-situ evaluation will be conducted within the Sydney based municipal sewer system. Eventually, the field results will be reported in the appropriate journal.

Acknowledgments

This publication is an outcome from the Data Analytics on Sewers Project funded by Sydney Water Corporation, Melbourne Water Corporation, Water Corporation (WA) and South Australian Water Corporation. The research participants are Data61-Commonwealth Scientific and Industrial Research Organization (CSIRO), University of Technology Sydney (UTS) and University of Newcastle (UoN).

References

[1] M Dunbabin and Marques L. Robotics for environmental monitoring. IEEE Robotics and Automation Magazine, 19:24–39, 2012.

[2] K Thiyagarajan and S Kodagoda. SMART monitoring of surface temperature and moisture content using multisensory data fusion. In 2015 IEEE 7th International Conference on Cybernetics and Intelligent Systems (CIS) and IEEE Conference on Robotics, Automation and Mechatronics (RAM), pages 222–227, 2015.

[3] Guangming Jiang, Jurg Keller, and Philip L Bond. Determining the long-term effects of H 2 S concentration, relative humidity and air temperature on concrete sewer corrosion. Water research, 65:157–169, 2014.

[4] Margarito Quintero-Núñez, Benjamin Valdez, and Michael Schorr. Effect of H2S on corrosion in polluted waters. In Advanced Materials Research, volume 95, pages 33–36. Trans Tech Publ, 2010.

[5] Gerhardus H Koch, Michiel P H Brongers, Neil G Thompson, Y Paul Virmani, and Joe H Payer. Corrosion cost and preventive strategies in the United States. Technical report, 2002.

[6] Esam Hewayde, M Nehdi, E Allouche, and G Nakhla. Effect of mixture design parameters and wetting-drying cycles on resistance of concrete to sulfuric acid attack. Journal of Materials in Civil Engineering, 19(2):155–163, 2007.

[7] B. Li, X. Fan, J. Zhang, Y. Wang, F. Chen, S. Kodagoda, T. Wells, L. Vorreiter, D. Vitanage, G. Iori, D. Cunningham, and T. Chen. Predictive Analytics Toolkit for H2S Estimation and Sewer Corrosion. In OZWater, Sydney, 2017. Australian Water Association.

[8] K Thiyagarajan, S Kodagoda, and N Ulapane. Data-driven machine learning approach for predicting volumetric moisture content of concrete using resistance sensor measurements. In 2016 IEEE 11th Conference on Industrial Electronics and Applications (ICIEA), pages 1288–1293, 2016.

[9] Karthick Thiyagarajan and Sarath Kodagoda. Analytical Model and Data-driven Approach for Concrete Moisture Prediction. In 33rd International Symposium on Automation and Robotics in Construction (ISARC 2016), pages 298–306, Auburn, 2016. IAARC.

[10] Ueli M. Angst and Bernhard Elsener. On the applicability of the wenner method for resistivity measurements of concrete. ACI Materials Journal, 2014.

[11] Sathira Wickramanayake Mudalige Don. Design and development of a resistivity measuring device for structural health monitoring. page 68, 2017.

[12] Linh V. Nguyen, Sarath Kodagoda, and Ravindra Ranasinghe. Spatial Sensor Selection via Gaussian Markov Random Fields. IEEE Transactions on Systems, Man, and Cybernetics: Systems, 2016.

[13] Carl Edward Rasmussen. Gaussian processes for machine learning. 2006.

[14] R Ranasinghe and S Kodagoda. Spatial prediction in mobile robotic wireless sensor networks with network constraints. In 2016 14th International Conference on Control, Automation, Robotics and Vision (ICARCV), pages 1–6. IEEE, 2016.

[15] L V Nguyen, S Kodagoda, R Ranasinghe, and G Dissanayake. Mobile robotic wireless sensor networks for efficient spatial prediction. 2014 IEEE/RSJ International Conference on Intelligent Robots and Systems, 2014.

[16] Finn Lindgren, HÃěvard Rue, and Johan Lindström. An explicit link between gaussian fields and gaussian markov random fields: The stochastic partial differential equation approach. Journal of the Royal Statistical Society. Series B: Statistical Methodology, 2011.

[17] Peter J Diggle and Paulo J Ribeiro Jr. An overview of model-based geostatistics. In Model-based Geostatistics. 2006.

[18] P.J. Diggle and P.J. Ribeiro Jr. Gaussian models for geostatistical data. Model-based Geostatistics, 2007.

[19] Finn Lindgren, HÃěvard Rue, and Johan Lindström. An explicit link between gaussian fields and gaussian markov random fields: The stochastic partial differential equation approach. Journal of the Royal Statistical Society. Series B: Statistical Methodology, 2011.

[20] Alfio Quarteroni and Alberto Valli. Numerical Approximation of Partial Differential Equations (Springer Series in Computational Mathematics). Springer Series in Computational Mathematics, 1996.

[21] C. M. Bishop. Pattern Recognition and Machine Learning. In Pattern Recognition and Machine Learning. 2006.

[22] Dennis S. Bernstein. Matrix mathematics: Theory, facts, and formulas with application to linear systems Theory, 2006.